

KEK-TH-939
 UCL-IPT-04-01
 hep-ph/0401246

Inclusive J/ψ Productions at e^+e^- Colliders

K. Hagiwara¹, E. Kou², Z.-H. Lin¹, C.-F. Qiao^{3,4}, G.-H. Zhu¹

¹ Theory Group, KEK, Tsukuba, Ibaraki 305-0801, Japan

² Institut de Physique Théorique, Université Catholique de Louvain,
 Chemin Cyclotron 2, B-1348 Louvain-la-Neuve, Belgium

³ CCAST(World Lab.), P.O. Box 8730, Beijing 100080, China

⁴ Dept. of Physics, Graduate School of the Chinese Academy of Sciences,
 YuQuan Road 19A, Beijing 100039, China

Abstract

Inclusive J/ψ productions in e^+e^- annihilation is studied in the framework of NRQCD. We first review the leading-order calculations of the cross sections for $e^+e^- \rightarrow J/\psi c\bar{c}$ and $e^+e^- \rightarrow J/\psi gg$ and find that their ratio is about 1:1.5 at $\sqrt{s} \simeq 10$ GeV. This result is in conflict with the current measurements by the Belle Collaboration, which finds that the process $e^+e^- \rightarrow J/\psi c\bar{c}$ accounts for about 2/3 of all the prompt J/ψ 's. We show that the discrepancy in the total rate as well as in the J/ψ momentum distributions can be resolved by considering a large renormalization K factor ($K \simeq 4$) for the $J/\psi c\bar{c}$ cross section and by taking into account collinear suppression in the end-point energy region of $J/\psi gg$ production. Detailed studies of the model predictions in terms of the density matrix are performed and various momentum and angular distributions are presented as functions of the K factors. These distributions can be used to determine the normalizations of each subprocess provided that the production and decay angular distributions do not alter much by higher order corrections.

PACS number(s): 12.38.Bx, 12.39.Jh, 13.60.Le, 14.40.Lb

1 Introduction

As one of the simplest processes to investigate both perturbative and nonperturbative properties of quantum chromodynamics (QCD), charmonium production at various collision processes has stimulated a lot of interesting theoretical and experimental works. One of such developments in the past few years, called nonrelativistic quantum chromodynamics (NRQCD) [1] which generalizes and improves the conventional color-singlet model (CSM), has provided a successful explanation of the CDF measurements of prompt J/ψ and ψ' production at the Tevatron [2]. Within the framework of NRQCD, the puzzle of ψ productions in excess of the CSM prediction can be solved by introducing significant contributions from color-octet terms, which correspond to a gluon forming a $c\bar{c}$ pair in a color-octet state at short distances and then evolving at long distances into a color-singlet state along with other light quarks. To confirm the validity of the color-octet mechanism (COM), Braaten and Chen first suggested that the inclusive ψ productions through e^+e^- annihilation may provide an opportunity to observe the color-octet contributions to the cross section and angular distributions [3]. Subsequently many detailed calculations have been performed in the literature [4, 5, 6, 7, 8, 9, 10].

Recently, BaBar and Belle Collaborations have published their experimental data for prompt J/ψ productions [11, 12, 13]. Both measurements for the inclusive processes are dramatically larger than the leading-order prediction of the CSM. However, there is no obvious evidence in support of the existence of the color-octet state reported by Belle measurement, especially in the upper end-point region of J/ψ momentum distributions where the significant color-octet signal is predicted by previous analysis. Although higher order corrections may significantly soften the hard J/ψ momentum spectrum of the COM [14], it is the following Belle observation

$$\sigma(e^+e^- \rightarrow J/\psi c\bar{c})/\sigma(e^+e^- \rightarrow J/\psi X) = 0.59^{+0.15}_{-0.13} \pm 0.12 = 0.59 \pm 0.18, \quad (1)$$

which prompts us to reconsider the normalization of the $J/\psi c\bar{c}$ production in CSM. Even higher ratio,

$$\sigma(e^+e^- \rightarrow J/\psi c\bar{c})/\sigma(e^+e^- \rightarrow J/\psi X) = 0.67 \pm 0.12, \quad (2)$$

has been reported by Belle as a preliminary result based on 86.7fb^{-1} data set [15]. Since it is unlikely that COM gives the ratio larger than a quarter, we may conclude that the COM contribution is sub-dominant in the process $e^+e^- \rightarrow J/\psi X$ at $\sqrt{s} = 10\text{ GeV}$.

In this report, we assume that the COM contribution is negligible for prompt J/ψ productions, and study if the CSM predictions for $e^+e^- \rightarrow J/\psi c\bar{c}$ and $e^+e^- \rightarrow J/\psi gg$ can be made consistent by introducing the renormalization K factors for the total cross sections, and by considering the softening of the J/ψ momentum spectrum in the $J/\psi gg$ process. We give predictions for the J/ψ production and decay angular distributions, which will be useful to test our assumptions and to measure the K factors and the momentum distributions of individual subprocesses in future precision experiments.

We note here some other evidences that may support our assumption indirectly. The exclusive cross sections for the double-charmonium productions such as $e^+e^- \rightarrow J/\psi\eta_c$, measured by Belle, is also one order of magnitude larger than the leading-order prediction [13]. Since in the exclusive processes, the color-octet contribution is negligible, a large K factor for the $e^+e^- \rightarrow J/\psi\eta_c$ production amplitude in the CSM may be necessary to explain the experimental data, as has been illustrated in Ref. [16].

Lately some authors have calculated electromagnetic contributions and the relativistic correction [17], and also considered the possibility of mis-detecting the QED process $e^+e^- \rightarrow J/\psi J/\psi$ at Belle [18, 19]. However, since the considered subprocesses have the same order of magnitude of the original tree-level cross section in CSM, they are not sufficient to provide an explanation of the large enhancement of the $J/\psi c\bar{c}$ cross section. In the recent report [20], Belle collaboration showed that they are capable of distinguishing J/ψ from η_c and that they observe no evidence of $e^+e^- \rightarrow J/\psi J/\psi$ yet.

Another evidence of possible suppression of COM comes from radiative Υ decays. At the amplitude level, $\Upsilon \rightarrow \gamma X$ is quite similar to inclusive J/ψ productions except for the heavy quark masses. Recently, radiative Υ decays observe by CLEO [21] has been studied in the framework of the combination of NRQCD and the soft-collinear effective theory (SCET) [22, 23]. The result shows that a good fit in the end-point region of the photon energy spectrum is obtained only when the color-octet matrix elements are set to zero. The same may or may not apply for prompt J/ψ production in e^+e^- collisions, but we can take into account the collinear suppression effect at the end-point region in $e^+e^- \rightarrow J/\psi gg$ process, which is very similar to that of the $\Upsilon \rightarrow \gamma gg$ in the CSM.

In Section 2, we give the leading-order calculations of the processes $e^+e^- \rightarrow J/\psi c\bar{c}$ and $e^+e^- \rightarrow J/\psi gg$ and correct some mistakes in literatures. The production of $J/\psi c\bar{c}$ through two virtual photons is also considered and the fractions for transversely and longitudinally polarized J/ψ are presented. In Section 3, we extract the collinear suppression effect in $e^+e^- \rightarrow J/\psi gg$ production from the photon momentum spectrum of Υ radiative decays, and find that the observed J/ψ momentum spectrum and the $J/\psi c\bar{c}$ fraction Eq.(2) can be reproduced by the CSM if we introduce a large K factor of $K \simeq 4$ for the $J/\psi c\bar{c}$ cross section while the $J/\psi gg$ process does not need a K factor significantly different from unity. In Section 4, we present various distributions for the inclusive J/ψ productions in the different momentum regions and study the sensitivity of the K factor in terms of several production and decay angular asymmetries. In Section 5, We discuss the connection between the inclusive process and the exclusive double-charmonium production. Finally, our conclusions are given in Section 6. In Appendix A, we present technical details of the scheme which we developed to calculate the helicity amplitudes of NRQCD processes by using the HELAS codes [24, 25].

2 The Leading-order Calculations

In the color-singlet picture, three production modes are involved in the inclusive J/ψ production processes, as shown in Fig. 1 and Fig. 2. We refer them to the QCD $J/\psi c\bar{c}$ produc-

tion (Fig. 1(a)), the QED $J/\psi c\bar{c}$ production (Fig. 1(b),(c),(d)) and the $J/\psi gg$ production (Fig. 2). Other QED processes such as $e^+e^- \rightarrow J/\psi\gamma^*$ where the γ^* forms a lepton or quark pair (except for the charm pair) have been regarded as the background and removed experimentally [12]. The $J/\psi gg$ production was initially investigated twenty years ago and was taken as the most important production mode in comparison with the color-octet production in the old-fashioned "color-evaporation model" [26]. The calculations on the QCD $J/\psi c\bar{c}$ production have been carried out in Refs. [4, 5, 6] and shows that the cross section is comparatively smaller than that of $J/\psi gg$ production. In the case of the t -channel QED $J/\psi c\bar{c}$ production (Fig. 1(b)), Ref. [9] shows that the cross section is only 1/6 of the QCD one and the modest effects are expected. Here in spite of a suppression factor α_{EM}^2/α_s^2 compared to the QCD $J/\psi c\bar{c}$ production, the t -channel diagrams of the QED $J/\psi c\bar{c}$ process should be taken into account due to the enhancement of powers of $\sqrt{s}/2m_c$, which is studied in detail in Refs. [7, 18, 9]. According to the Furry's theorem, the density matrix of the interferences between s - and t - channel $J/\psi c\bar{c}$ processes (including the s - channel QCD diagrams) vanishes when $c\bar{c}$ angular distributions in the $c\bar{c}$ rest frame are integrated out. We also calculate the corrections from s -channel QED productions (the detailed procedures of our calculations will be shown later)

$$\begin{aligned} \frac{|a+c|^2 - |a|^2}{|a|^2} &= -3.0\% + 3.5 \times 10^{-3}, \\ \frac{|a+d|^2 - |a|^2}{|a|^2} &= 2.0\% + 1.0 \times 10^{-4}, \end{aligned} \quad (3)$$

where the symbols $|a|^2, |c|^2, |d|^2$ represent the contributions to the total cross section from diagrams Fig. 1(a), (c) and (d), respectively. The first values on the right-hand side of Eq. (3) represent the corrections from the interference terms $2\text{Re}(ac^*)/|a|^2$ and $2\text{Re}(ad^*)/|a|^2$, while the second values represent the direct corrections $|c|^2/|a|^2$ and $|d|^2/|a|^2$. We note that the interference between the diagrams (a) and (c) is negative, which is consistent with the QED corrections to the exclusive process $e^+e^- \rightarrow J/\psi\eta_c$ [17]. As expected, the sum of the above corrections from the s -channel QED processes contributes to the total $J/\psi c\bar{c}$ cross section destructively by about 1%, which is sufficiently small and can be neglected safely. Therefore, in the rest of the paper, we refer only to the t -channel QED $J/\psi c\bar{c}$ production of Fig1. (b) as the QED process.

It has been noted that the color-octet process $e^+e^- \rightarrow [c\bar{c}]_8 g \rightarrow J/\psi g$ exhibits a remarkably different property with all of the above three color-singlet productions. This process gives rise to a hard spectrum where the J/ψ momentum is almost maximal because of its two-body final state [3]. This has been a crucial feature used in experiments to distinguish the color-octet contributions. As mentioned in the last section, no such signature has been detected by BaBar [11] and Belle [12, 13]. Recent investigation reveals that the color-octet contribution to the J/ψ spectrum can be broaden significantly by the large perturbative corrections and enhanced nonperturbative effects [14]. In this sense, one cannot rule out the color-octet contribution from current experimental data yet. However, as concluded in Ref. [14], due to the unknown color-octet shape functions for the J/ψ production, the dom-

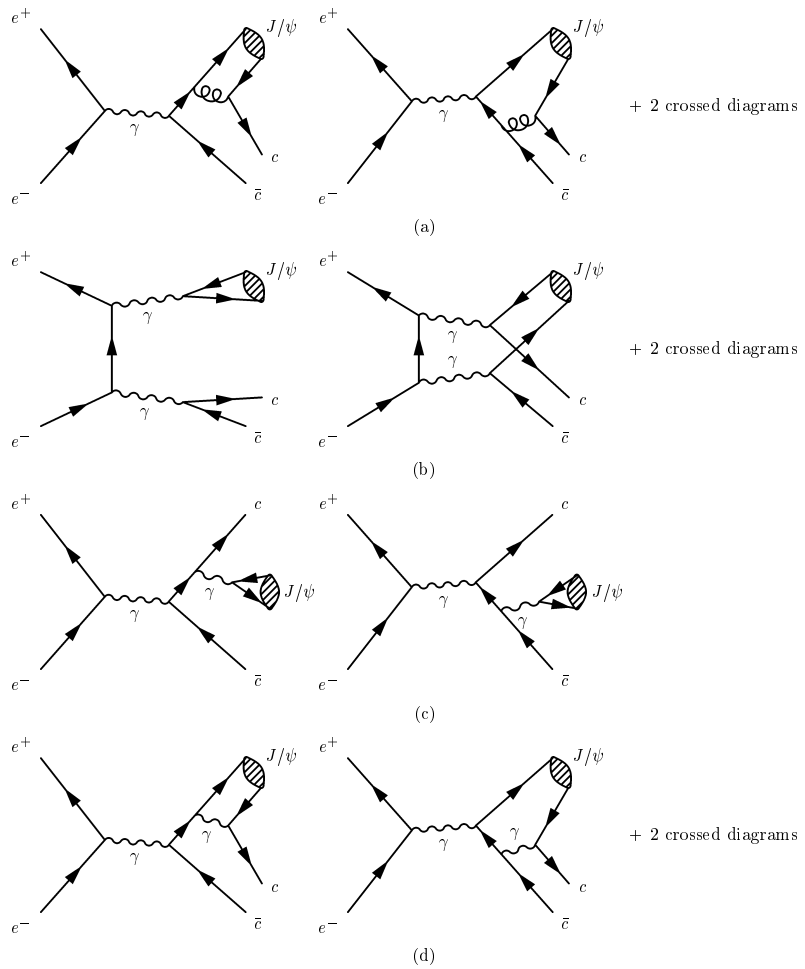


Figure 1: Feynman diagrams for the $J/\psi c\bar{c}$ productions from $e^+ + e^-$ annihilation: (a) the QCD production, (b) the t -channel QED production, (c) and (d) the s -channel QED productions.

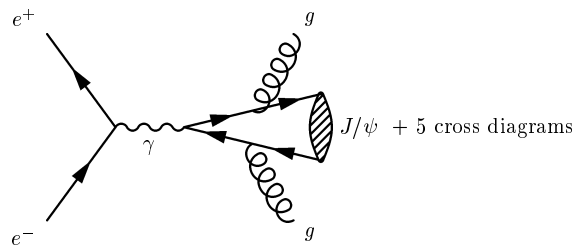


Figure 2: Feynman diagrams for the $J/\psi gg$ production from $e^+ + e^-$ annihilation.

inant $J/\psi c\bar{c}$ cross section must be understood accurately before extracting the color-octet contributions from the data.

We now present our leading-order calculations. The traditional approach for S -wave productions is either calculating the helicity amplitudes by using a covariant projection formalism in the CSM, or evaluating the squared amplitudes directly with the help of the optical theorem in the general NRQCD factorization framework. To the lowest order in the power expansion in the relativistic velocity v of the heavy quark and anti-quark, the two methods are identical with each other. In this paper, we develop a much simpler numerical method for the amplitude calculations. First we apply the program MadGraph [25] to generate the parton-level helicity amplitudes for the processes $e^+e^- \rightarrow c\bar{c}c\bar{c}$ and $e^+e^- \rightarrow c\bar{c}gg$, and then combine a color-singlet $c\bar{c}$ pair to be a J/ψ meson by using the HELAS subroutines [24]. We leave the detailed procedure for constructing the helicity amplitudes for NRQCD processes in the appendix. Finally the integration over the phase space of the squared amplitudes are performed by the Monte Carlo program BASES [27]. This approach avoids lengthy trace computations and allows us to obtain various production and decay angular distributions from the density matrices that can easily be obtained from the helicity amplitudes.

In our numerical analysis we use the input parameter values as follows: the center-of-mass energy $\sqrt{s} = 10.58$ GeV, $m_c = 1.5$ GeV, $\alpha_s(2m_c) = 0.258$, and $\alpha_{EM}(2m_c) = 1/129.6$. The radial wave function for J/ψ at the origin $R(0)$ is measured through the leptonic decay width $\Gamma(J/\psi \rightarrow e^+e^-)$,

$$|R(0)|^2 = \frac{9M_{J/\psi}^2}{16\alpha_{EM}^2} \Gamma(J/\psi \rightarrow e^+e^-) = 0.447 \text{ GeV}^3, \quad (4)$$

where $\Gamma(J/\psi \rightarrow e^+e^-) = 5.26 \times 10^{-6}$ GeV, and $M_{J/\psi} \simeq 2m_c$. Here we adopt the $R(0)$ value obtained from the above leading-order formula, rather than from the next-to-leading-order one [17] or from some potential models [28], in order to define the renormalization K factor of the J/ψ production cross section unanimously.

With the above parameters, the leading-order cross sections for the inclusive J/ψ processes are given as

$$\begin{aligned} \sigma_{cc}^{QCD} &= 0.0897 \text{ pb} \quad \text{for the QCD } J/\psi c\bar{c} \text{ production,} \\ \sigma_{cc}^{QED} &= 0.0156 \text{ pb} \quad \text{for the QED } J/\psi c\bar{c} \text{ production,} \\ \sigma_{gg} &= 0.162 \text{ pb} \quad \text{for the } J/\psi gg \text{ production.} \end{aligned} \quad (5)$$

The ratio for the configurations of $J/\psi c\bar{c}$ and $J/\psi gg$, *i.e.* $(\sigma_{cc}^{QCD} + \sigma_{cc}^{QED})/\sigma_{gg}$, is about 1:1.5, while $\sigma_{cc}^{QCD}/\sigma_{gg} = 1 : 1.8$, which are much larger than the previous results given in Refs. [4, 5, 6]. For σ_{cc}^{QCD} , choosing the same input values used in Refs. [4, 5, 6], our result agrees with Ref. [6] but disagrees with that in Ref. [5] and is three times larger than that in Ref. [4]. This missing factor 3 was also pointed out in Ref. [6]. In the case of σ_{gg} , our result is smaller than those in Refs. [4, 6] by about a factor of 2, but is consistent with that in Refs. [26]. In addition, our result for σ_{cc}^{QED} agrees with that in Ref. [9]. Both σ_{cc}^{QCD} and σ_{gg} contribute

to the total inclusive cross section at $O(\alpha_s^2 \alpha_{EM}^2)$, while σ_{cc}^{QED} contributes at $O(\alpha_{EM}^4)$. The QED cross section is enhanced by powers of $\sqrt{s}/2m_c$. As we shall see, the contribution from the QED $J/\psi c\bar{c}$ production affects the angular distributions significantly at larger J/ψ momenta.

We also examine the consistency of our numerical results with the fragmentation approximation in the high energy limit; $\sqrt{s} \gg 2m_c$. In Ref. [29], the charm quark fragmentation function into J/ψ has been defined as

$$\mathcal{D}_{c \rightarrow J/\psi}(x) = \lim_{s \rightarrow \infty} \frac{1}{2 \sigma(e^+e^- \rightarrow c\bar{c})} \frac{d\sigma^{QCD}}{dx}(e^+e^- \rightarrow J/\psi c\bar{c}) \quad (6)$$

and is found to be

$$\mathcal{D}_{c \rightarrow J/\psi}(x) = \frac{8}{27\pi} \alpha_s (2m_c)^2 \frac{|R(0)|^2}{m_c^3} \frac{x(1-x)^2(16-32x+72x^2-32x^3+5x^4)}{(2-x)^6} \quad (7)$$

with $x = 2E_{J/\psi}/\sqrt{s}$ ($E_{J/\psi}$ is the J/ψ energy). We confirm the above result numerically and find that the deviation between the fragmentation formula (7) and the exact differential cross section decreases as m_c/\sqrt{s} at high energies. The difference is about 6.2% at $\sqrt{s} = 50$ GeV and 2.4% at $\sqrt{s} = 100$ GeV.

In Fig. 3, we show the momentum and angular distributions for the three types of J/ψ productions. Throughout the paper, we adopt a dimensionless variable z for the J/ψ momentum distributions. The relation between z and the J/ψ momentum $P_{J/\psi}$ is given by $z = P_{J/\psi}/P_{J/\psi}^{max}$, where $P_{J/\psi}^{max}$ denotes the maximum value of the J/ψ momentum in the inclusive J/ψ processes, namely, $P_{J/\psi}^{max} = (s - M_{J/\psi}^2)/2\sqrt{s} \simeq 4.86$ GeV. For $e^+e^- \rightarrow J/\psi c\bar{c}$, $P_{J/\psi}$ cannot achieve $P_{J/\psi}^{max}$ due to the kinematic constraint. The largest $P_{J/\psi}$ is $\sqrt{s/4 - 4m_c^2}$ which is about 4.36 GeV, corresponding to $z \simeq 0.90$ at $\sqrt{s} = 10.58$ GeV. In the case of angular distributions, we define θ as the opening angle between the produced J/ψ momentum and the electron beam. Both z and θ are defined in the e^+e^- collision center-of-mass frame.

From Fig. 3(a) and (b), we observe that although the QED $J/\psi c\bar{c}$ cross section is much smaller than the QCD one, its effects in the high momentum region and at large $|\cos \theta|$ cannot be neglected. This is due to the characteristics of the photon fragmentation diagrams where one virtual photon fragments into a charmonium and another one evolves into a $c\bar{c}$ pair (see the left-most Feynman diagram in Fig. 1(b)). The photon fragmentation configurations make up 71% of the QED cross section, while the rest comes from the interference terms and non-fragmentation terms. In the end-point region $0.9 < z < 1$, only the $J/\psi gg$ mode is allowed.

The differential cross sections for the QCD $J/\psi c\bar{c}$ and the $J/\psi gg$ productions are restricted by unitarity, parity, and angular momentum considerations and can be parameterized to a simple form [4]

$$\frac{d^2\sigma}{dz d\cos \theta} = S(z)[1 + \alpha(z) \cos^2 \theta], \quad (8)$$

where the angular coefficient $\alpha(z)$ is generally limited in the interval $-1 \leq \alpha(z) \leq 1$. The angular distributions of the QCD $J/\psi c\bar{c}$ process (denoted by solid curves) in Fig. 3(b) gives a positive α ($\alpha \sim 0.46$), corresponding to the dominance of transverse J/ψ mesons, while the flat shape of the $J/\psi gg$ angular distribution (dotted lines) gives $\alpha \sim 0$, corresponding to a large fraction of the longitudinally polarized J/ψ ($\sigma_L/\sigma_T \sim 1.8$). These features can be confirmed in Fig. 3(c) and (d), where we show the fraction of transversally polarized J/ψ as function of z and $\cos\theta$, respectively. In contrast to the above cosine-square behavior in Eq. (8), the differential cross section for the QED $J/\psi c\bar{c}$ production has strong enhancement near $|\cos\theta| \sim 1$ because of the t -channel electron exchange amplitude, Fig. 1(b).

The fraction of the transversely polarized J/ψ is displayed in Fig. 3(c) and (d) where the transverse cross sections have been normalized by the respective total cross sections for the three production modes. For the $J/\psi c\bar{c}$ mode, both the QCD and QED cross sections are dominated by the transverse J/ψ , and the transverse J/ψ fraction increases with the J/ψ momentum. On the other hand, an opposite behavior is obtained for $J/\psi gg$. We point out here that the transverse fraction for the QCD $J/\psi c\bar{c}$ production approaches to unity as z reaches 0.90, the maximum for the process. This feature is not clearly seen in Fig. 3(c) due to the finite bin size, but has been checked numerically. It indicates that all J/ψ mesons are transversely polarized if the associated $c\bar{c}$ has vanishing relative momentum. This is consistent with the exclusive double-charmonium production $e^+e^- \rightarrow J/\psi\eta_c$ where all J/ψ mesons are transversely polarized. The scattering-angle distributions are also quite distinct from each other; as shown in Fig. 3(d). In the region of the small scattering angles, the transverse components for the QCD $J/\psi c\bar{c}$ and $J/\psi gg$ processes are comparatively larger than those in the large-angle region. For the QED $J/\psi c\bar{c}$ process, the transverse fraction rapidly falls off in the region $|\cos\theta| > 0.8$.

3 The Collinear Suppression and K Factors

We note that although the contribution from the $J/\psi gg$ process is significant in the end-point region $0.90 < z < 1$ in our leading-order calculations, there is no such apparent signal observed by experiments. The probable reason of this discrepancy is that NRQCD does not include collinear degrees of freedom at large z and therefore both the perturbative expansion and the operator product expansion (OPE) break down [30]. The problem can be cured by combining NRQCD for the heavy degrees of freedom with the soft-collinear effective theory (SCET) for the light degrees of freedom [31]. A similar problem occurs in the radiative decay $\Upsilon \rightarrow \gamma gg$ at large γ energies as mentioned in Sec. 1. In Refs. [23], it has been shown that the prediction of SCET in the end-point region of the γ energy distribution is much closer to the CLEO data than the leading-order calculations in NRQCD.

In this paper instead of performing the complicated calculations within SCET, we adopt a phenomenological approach to obtain an appropriate end-point spectrum for the $J/\psi gg$ process by noting that in SCET, the operator of $\gamma^* \rightarrow J/\psi gg$ is in the same form as that of $\Upsilon \rightarrow \gamma gg$. It is further observed that, the collinear Sudakov factor of Υ decay arises solely from the gluon jet function. In the leading power expansion of SCET, the jet function

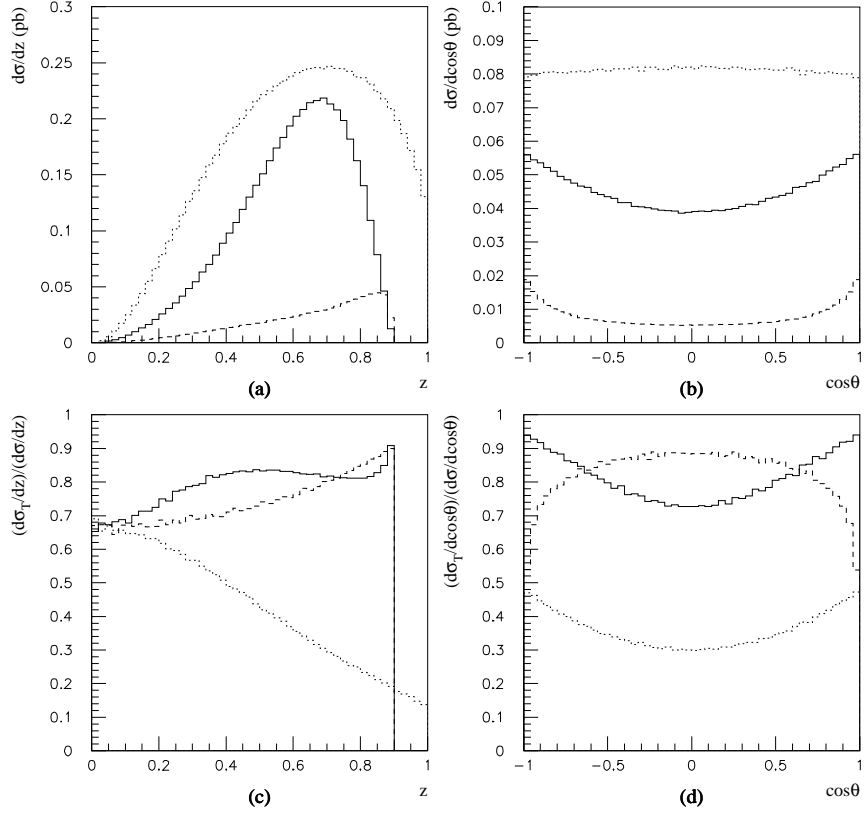


Figure 3: Momentum and angular distributions of $e^+e^- \rightarrow J/\psi c\bar{c}$ and $J/\psi gg$ processes: (a) and (b) are for the total cross section, and (c) and (d) are for the fraction of the transversely polarized J/ψ production. The solid, dashed and dotted lines correspond to the QCD $J/\psi c\bar{c}$, QED $J/\psi c\bar{c}$, and $J/\psi gg$ production, respectively.

depends only on the large light-cone momentum component. It is easy to find that, the large momentum component of two-gluon jet of $\Upsilon \rightarrow \gamma gg$ decay (M_Υ) is roughly equal to that of $\gamma^* \rightarrow J/\psi gg$ process ($(s - M_{J/\psi}^2)/\sqrt{s}$). This implies that the collinear Sudakov factor of these two processes are quite similar. Therefore it should be a reasonable approximation that these two processes have the same collinear suppression function.

Accordingly, we disentangle the collinear suppression function $F(z')$ from the experimental data and the tree level prediction for $\Upsilon \rightarrow \gamma gg$ as ^{*}

$$\frac{d\Gamma_{exp}}{dz'} = F(z') \times \frac{d\Gamma_{LO}}{dz'}, \quad (9)$$

where Γ_{exp} and Γ_{LO} are the decay width for the experimental measurement and the leading-order calculation respectively. z' is the normalized photon energy and can be expressed as a function of the invariant mass of the two gluons

$$z' = \frac{2E_\gamma}{M_\Upsilon} = 1 - \frac{M_{gg}^2}{M_\Upsilon^2}. \quad (10)$$

We assume that the function $F(z')$ can be parameterized as

$$F(z') = \begin{cases} 1 & \text{for } 0 \leq z' \leq 0.5 \\ (1 - z')\exp(c_1 z' + c_2 z'^2) & \text{for } 0.5 < z' \leq 1 \end{cases} \quad (11)$$

with two free parameters c_1 and c_2 . We find a good fit to the data and by using the LO calculation presented in Ref. [23], for

$$c_1 = 0.96, \quad c_2 = 0.69. \quad (12)$$

The suppression function in Eq. (11) shows that the collinear effects in the region $0 \leq z' \leq 0.5$ are negligible, the large suppression takes place in the end-point region $0.5 < z' \leq 1$. With Eqs. (11) and (12), the suppression effects in the Υ radiative decay can be well described. Finally, we obtain the modified differential cross section for $e^+e^- \rightarrow J/\psi gg$

$$\frac{d\sigma_{gg}}{z} = F \left(\sqrt{z^2 + \frac{4M_{J/\psi}^2}{s}} \right) \times \frac{d\sigma_{gg}^{LO}}{dz}, \quad (13)$$

where we replace the photon energy fraction z' by the J/ψ energy fraction $2E_{J/\psi}/\sqrt{s} = \sqrt{z^2 + 4M_{J/\psi}^2}/s$. We expect that this is a good approximation because the energy scale of the two processes is roughly the same. Integrating over z , the total cross section is reduced to

$$\sigma_{gg} = 0.123 \text{ pb}, \quad (14)$$

^{*}We obtain the experimental data and the tree level prediction from Fig. 3 in the first reference in Refs. [23].

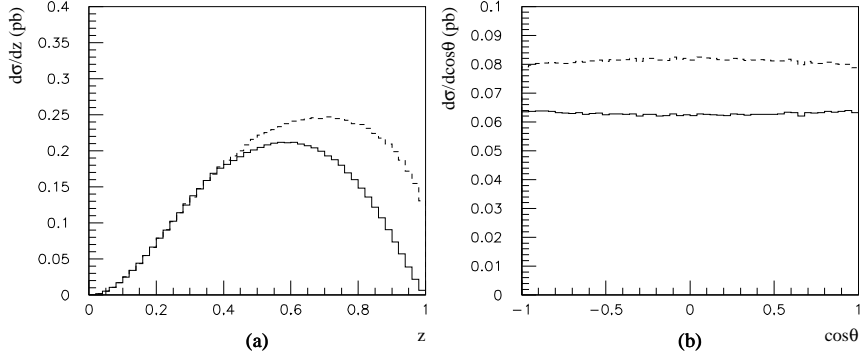


Figure 4: Momentum (a) and angular (b) distributions for the $J/\psi gg$ cross section. The dashed line is for the leading order calculation, while the solid line is for the calculation with the collinear suppression.

which is about 24% smaller than the original value in Eq. (5).

The end-point suppression behavior is plotted in Fig. 4(a) by the solid line, while the result of the leading order calculation is shown by the dashed line for comparison. In terms of the momentum fraction variable z , the suppression effect starts at around $z = 0.4$. As z is close to unity, the differential cross section drops to zero, which diminishes the disagreement with the Belle data. The angular distribution is modified slightly, as shown in Fig. 4(b). The cross section in the central region ($\cos\theta \sim 0$) is suppressed most because that the large z component dominated by the longitudinally polarized J/ψ mesons is suppressed significantly. After the collinear suppression factor is introduced, there is no apparent disagreement between the Belle data at large z and the NRQCD production of the $J/\psi gg$ process, without introducing a further overall suppression factor.

The NRQCD prediction for the direct $J/\psi c\bar{c}$ production is however significantly smaller than the Belle data. The prompt $J/\psi c\bar{c}$ production cross section obtained by Belle is $\sigma_{prompt} = (0.87^{+0.21}_{-0.19} \pm 0.17)$ pb based on D^{*+} and D^0 measurements [13]. Because the prompt J/ψ data contain contributions from the $\psi(2S) \rightarrow J/\psi$ transitions, we estimate the direct $J/\psi c\bar{c}$ production cross section as follows. Working in the framework of NRQCD, we find that direct $\psi(2S)c\bar{c}$ and $J/\psi c\bar{c}$ cross sections are proportional to the meson wave functions at the origin, and to the leptonic decay widths of $\psi(2S)$ and J/ψ . According to Eq. (4), we have

$$\sigma_{dir}(\psi(2S)c\bar{c}) : \sigma_{dir}(J/\psi c\bar{c}) = M_{\psi(2S)}^2 \Gamma(\psi(2S) \rightarrow e^+e^-) : M_{J/\psi}^2 \Gamma(J/\psi \rightarrow e^+e^-). \quad (15)$$

By using $\Gamma(\psi(2S) \rightarrow e^+e^-) = 2.15 \times 10^{-6}$ GeV and the branching ratio for the $\psi(2S) \rightarrow$

$J/\psi X$ transition fraction $B = 55.7\%$ [32], we obtain the direct $J/\psi c\bar{c}$ cross section

$$\begin{aligned}\sigma_{dir}(J/\psi c\bar{c}) &= \sigma_{prompt} \left[1 + B(\psi(2S) \rightarrow J/\psi X) \times \frac{M_{\psi(2S)}^2 \Gamma(\psi(2S) \rightarrow e^+e^-)}{M_{J/\psi}^2 \Gamma(J/\psi \rightarrow e^+e^-)} \right]^{-1} \\ &\simeq 0.66 \pm 0.26 \text{ pb.}\end{aligned}\quad (16)$$

Here we estimate the error of σ_{dir} from the statistical and systematic errors of σ_{prompt} . Comparing with the result given in Eq. (5), $\sigma_{cc}(J/\psi c\bar{c}) = \sigma_{cc}^{QCD} + \sigma_{cc}^{QED} = 0.11 \text{ pb}$, there is still a large gap between the experimental central value and the theoretical prediction. Moreover, the rate of $\sigma_{cc}/(\sigma_{cc} + \sigma_{gg})$ is about 0.46 evaluated from Eqs. (5) and (14), much smaller than the current experimental measurement 0.67 ± 0.12 in Eq. (2) as indicated in Sec. 1.

According to the argument given in the first section, the possible source of the disagreement may arise from the large higher-order corrections to the QCD $J/\psi c\bar{c}$ production process. For instance, if we set as K factor to unity for both QED $J/\psi c\bar{c}$ and $J/\psi gg$ processes, the direct $J/\psi c\bar{c}$ cross section in Eq. (16) requires a K factor for the QCD $J/\psi c\bar{c}$ production to be

$$K = 7.2 \pm 2.9, \quad (17)$$

while the fraction of the $J/\psi c\bar{c}$ process in Eq. (2) gives rise to

$$K = 2.6_{-1.1}^{+2.4}. \quad (18)$$

To fit to both the cross section and the fraction, we set the K factor to a moderate value 4 for the QCD $J/\psi c\bar{c}$ process, and then find

$$\sigma_{cc} = K \sigma_{cc}^{QCD} + \sigma_{cc}^{QED} = 0.374 \text{ pb}, \quad \sigma_{cc}/(\sigma_{cc} + \sigma_{gg}) = 75\%. \quad (19)$$

A part of the large K factor may come from the uncertainty in the wave function at the origin. By replacing the leading-order formula of the leptonic J/ψ decay in Eq. (4) by the next-to-leading-order one, the value of the wave function $|R(0)|^2$ is changed to be 0.792 GeV³ [17], while the wave function from some potential models is even larger, such as 0.810 GeV³ [28]. Because the cross section is proportional to $|R(0)|^2$, this effect gives the K factor of $792/447 \sim 1.77$ and $810/447 \sim 1.81$ respectively. Another factor of two from the higher-order corrections to the hard scattering part may lead to the combined effect as large as $K \sim 4$. For the QED $J/\psi c\bar{c}$ case, since the fragmentation configurations are dominant, the ratio $\sigma_{cc}^{QED}/\Gamma(J/\psi \rightarrow e^+e^-)$ is approximately a constant to any order of QCD perturbation theory. For this reason we choose the corresponding K factor to be equal to one. The $J/\psi gg$ cross section can also be enlarged by a factor of two caused by the the next-to-leading-order value of $|R(0)|^2$, but the higher-order QCD corrections of the hard part is unknown. For simplification and consistency with experimental data we set its K factor to be about one.

We emphasize here that only the qualitative aspects of the above discussions on the K factors should be taken seriously. The K factors should be calculated explicitly, and the predictions should be confronted against experiments. In the next section we show how to distinguish the contributing subprocesses experimentally.

4 Spin Density Matrix and Sensitivity to K Factors

In this section, we give more detailed analyses on the elements of the spin density matrix and various distributions.

Since the J/ψ mesons are reconstructed experimentally by using the leptonic decays $J/\psi \rightarrow \mu^+\mu^-, e^+e^-$, we describe the decay processes in the J/ψ rest frame by the polar and the azimuthal angle, θ^* and ϕ^* . The polar axis is chosen along the J/ψ momentum in the e^+e^- c.m. frame. The reduced helicity amplitudes for $e^+e^- \rightarrow J/\psi X$ are denoted by M_λ , where $\lambda = +1, 0, -1$ is the J/ψ helicity. Other particle's helicities are unobserved (integrated out) here. Then the production density matrix can be expressed as $R_{\lambda\lambda'} = \sum M_\lambda M_{\lambda'}^*$, where the summation is over the other particle helicities and momenta. For $e^+e^- \rightarrow J/\psi X \rightarrow l^+l^-X$, the differential cross section can be expressed as

$$\begin{aligned} & \frac{d\sigma_{total}}{dz d\cos\theta d\cos\theta^* d\phi^*} \\ = & \frac{3}{4\pi} \left\{ (R_{++} + R_{--}) \frac{1}{4} (1 + \cos^2\theta^*) + R_{00} \frac{1}{2} (1 - \cos^2\theta^*) \right. \\ + & 2\text{Re}(R_{+0} - R_{0-}) \frac{1}{4\sqrt{2}} \sin 2\theta^* \cos \phi^* - 2\text{Im}(R_{+0} - R_{0-}) \frac{1}{4\sqrt{2}} \sin 2\theta^* \sin \phi^* \\ + & \left. 2\text{Re}(R_{+-}) \frac{1}{4} \sin^2\theta^* \cos 2\phi^* - 2\text{Im}(R_{+-}) \frac{1}{4} \sin^2\theta^* \sin 2\phi^* \right\}. \end{aligned} \quad (20)$$

Here $R_{\lambda\lambda'}$ are the functions of z and $\cos\theta$ and we use the normalization $d\sigma_{total}/dz d\cos\theta = (R_{++} + R_{--} + R_{00})$ after integrating over $\cos\theta^*$ and ϕ^* . From Eq. (20), one can find that there are six independent combinations of the density matrix elements for the J/ψ productions that can be measured through the decay-lepton angular distributions.

According to the above common form, we calculate the different density matrix elements for all J/ψ inclusive processes and find that two of them $\text{Im}(R_{+0} - R_{0-})$ and $\text{Im}(R_{+-})$ vanish after integration over the unobserved internal momenta of $c\bar{c}$ or gg system because of CP invariance. Among the surviving four terms, $(R_{++} + R_{--})$ is actually the cross section for the transversely polarized J/ψ and R_{00} is for the longitudinally polarized J/ψ . After integrating over z and $\cos\theta$, three of them survive

$$\begin{aligned} \sigma_L &= \int R_{00} dz d\cos\theta, \\ \sigma_T &= \int (R_{++} + R_{--}) dz d\cos\theta, \\ \sigma_{+-} &= \int 2\text{Re}(R_{+-}) dz d\cos\theta. \end{aligned} \quad (21)$$

where $\sigma = \sigma_L + \sigma_T$ is the total cross section. We also note that σ_{+-} is from the nondiagonal spin density matrix elements and should be measured through the azimuthal angle of the decay leptons. The term proportional to $\text{Re}(R_{+0} - R_{0-})$ vanished after integration over $\cos\theta$.

We plot the momentum and angular distributions for σ , σ_T and σ_{+-} respectively in Fig. 5. The solid lines are for the sum of QCD and QED $e^+e^- \rightarrow J/\psi c\bar{c}$ processes, where we

set $K = 4$ factor for the QCD process. The dashed lines represent the $e^+e^- \rightarrow J/\psi gg$ contribution where the collinear suppression factor has been included. The dotted lines show their sum, the total J/ψ inclusive cross sections. Due to its large K factor, the $J/\psi c\bar{c}$ contribution is now dominant. Therefore, as shown in Fig. 5(a), our prediction of the total differential cross section versus the J/ψ momentum is roughly consistent with the experimental observation. The small but finite contribution from the $J/\psi gg$ process at $z > 0.9$ should eventually be observed by experiments, and its magnitude will constrain the K factor for the $J/\psi gg$ process for which we set $K = 1$ in our calculation. From Fig. 5(b), we see that the $J/\psi c\bar{c}$ mode prefers large $|\cos\theta|$, while the $J/\psi gg$ mode gives rather flat $\cos\theta$ distribution. Comparing with the transverse fractions for the QCD $J/\psi c\bar{c}$ process displayed in Fig. 3(c) and (d), we find those for the summed $J/\psi c\bar{c}$ mode in Fig. 5(c) and (d) are changed only slightly because of the large K factor for the QCD process. In the region $|\cos\theta| > 0.9$, the small suppression from the QED $J/\psi c\bar{c}$ component is observed. The nondiagonal element σ_{+-} is quite different for $J/\psi c\bar{c}$ and $J/\psi gg$, in particular at large z where σ_{+-} has the opposite signs. Since σ_{+-} is the coefficient of $\cos 2\phi^*$ depicted in Eq. (20), it should approach zero as the direction of the J/ψ momentum is along the beamline, *i.e.* $|\cos\theta| = 1$. It can be seen from the angular distributions for σ_{+-} plotted in Fig. 5(f).

In Fig. 6, we extend our above analyses on the angular distributions for different momentum regions: $0 \leq z \leq 0.4$ (1-a,b,c), $0.4 < z \leq 0.7$ (2-a,b,c) and $0.7 < z \leq 1$ (3-a,b,c), corresponding to $0 \leq P_{J/\psi} \leq 1.94$ GeV, 1.94 GeV $< P_{J/\psi} \leq 3.40$ GeV and 3.40 GeV $< P_{J/\psi} \leq 4.86$ GeV, respectively. The angular distribution of the total cross section $d\sigma/d\cos\theta$ is given in the figures (1-a,2-a,3-a), where the $J/\psi gg$ contribution is almost flat at all z region, and the contribution from the $J/\psi c\bar{c}$ process is more pronounced at large $|\cos\theta|$. The ratio of $d\sigma/d\cos\theta$ at $|\cos\theta| = 1$ and $\cos\theta = 0$ is about 1.3 at small z (1-a), 1.5 at medium z (2-a), and 1.7 at large z (3-a) for the $J/\psi c\bar{c}$ contribution. The fractions of the transverse cross section $d\sigma_T/d\cos\theta$ and the total distribution are shown in the figures (1-b,2-b,3-b). The $J/\psi c\bar{c}$ contribution has generally large σ_T/σ ratio, greater than about 0.7, at all $\cos\theta$ and z regions, while the $J/\psi gg$ contribution gives smaller ratio, especially at large angles and large z . It should also be noted that the $\cos\theta$ dependence of the σ_T/σ ratio for $J/\psi c\bar{c}$ process is sensitive to the K factor for the QCD process, because the QCD and QED subprocesses have very different $\cos\theta$ distribution, as shown in Fig. 3(d). The fractions of $\sigma_{+-}/d\cos\theta$ are displayed in the figures (1-c,2-c,3-c). Similar with the distributions in Fig. 5(f), the fraction of $\sigma_{+-}/d\cos\theta$ is zero at $|\cos\theta| = 1$. For the $J/\psi gg$ contribution, the maximum value of the fraction of $\sigma_{+-}/d\cos\theta$ appears at $\cos\theta = 0$ and is about 0.08 at small z (1-c), 0.04 at medium z (2-c), and 0.03 at large z (3-c). For the $J/\psi c\bar{c}$ contribution, the fraction of $\sigma_{+-}/d\cos\theta$ at $\cos\theta = 0$ is about 0.22, 0.12 and -0.02 at small z (1-c), medium z (2-c) and large z (3-c) respectively. At large z (3-c), the fraction of $\sigma_{+-}/d\cos\theta$ is negative due to the large contributions from the QED $J/\psi c\bar{c}$ process. Summing up, the angular distributions for the $J/\psi c\bar{c}$ and $J/\psi gg$ are significantly different in the various momentum regions.

The results of Fig. 5 and Fig. 6 are shown for $K = 4$ for the QCD $J/\psi c\bar{c}$ production. Since the actual value of K is still uncertain ($K = 7.2 \pm 2.9$ from $\sigma_{dir}(J/\psi c\bar{c})$, and $K = 2.6^{+2.4}_{-1.1}$ from $\sigma(J/\psi c\bar{c})/\sigma(J/\psi X)$ as shown in Eqs. (17) and (18)), we study the sensitivity of various

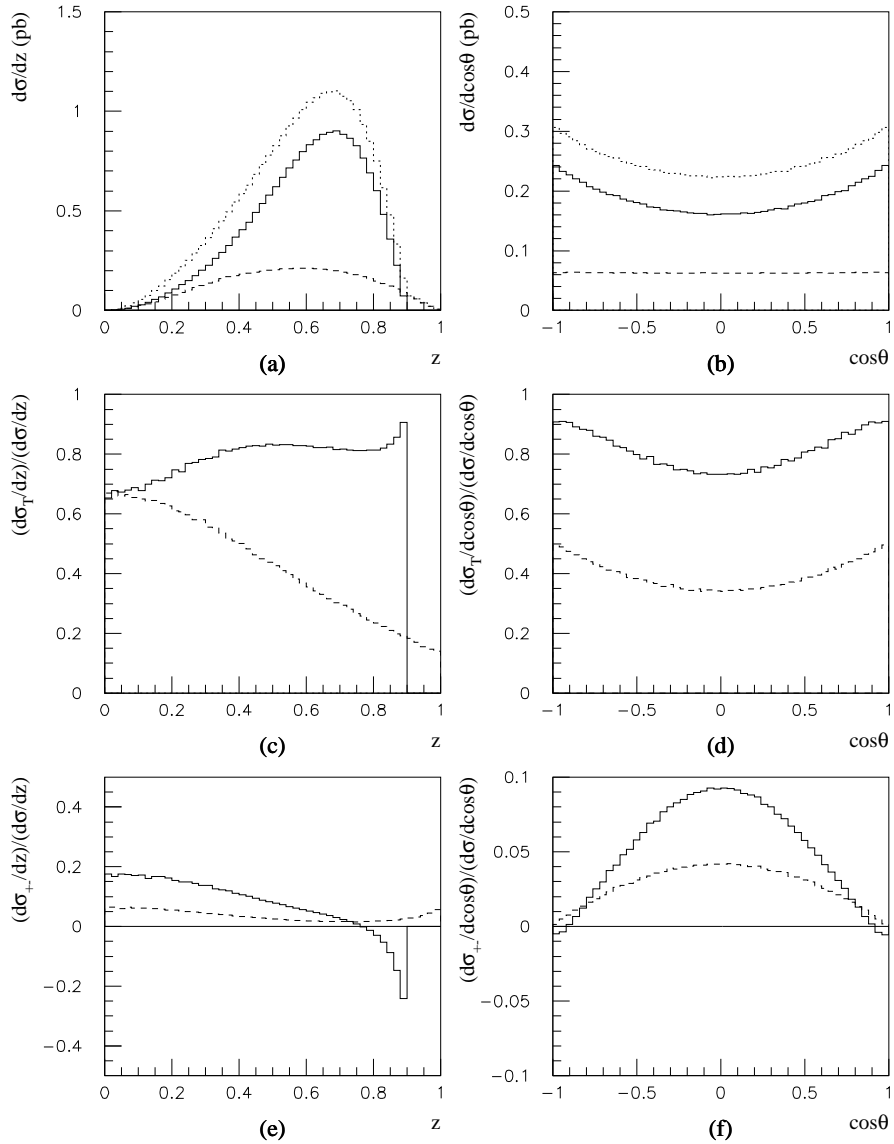


Figure 5: Momentum and angular distributions: (a) and (b) are for the total cross section, and (c) and (d) are for the fraction of the transversely polarized J/ψ , (e) and (f) are for the fraction of σ_{+-} . The solid, dashed and dotted lines correspond to the $J/\psi cc$, $J/\psi gg$ and total inclusive productions respectively.

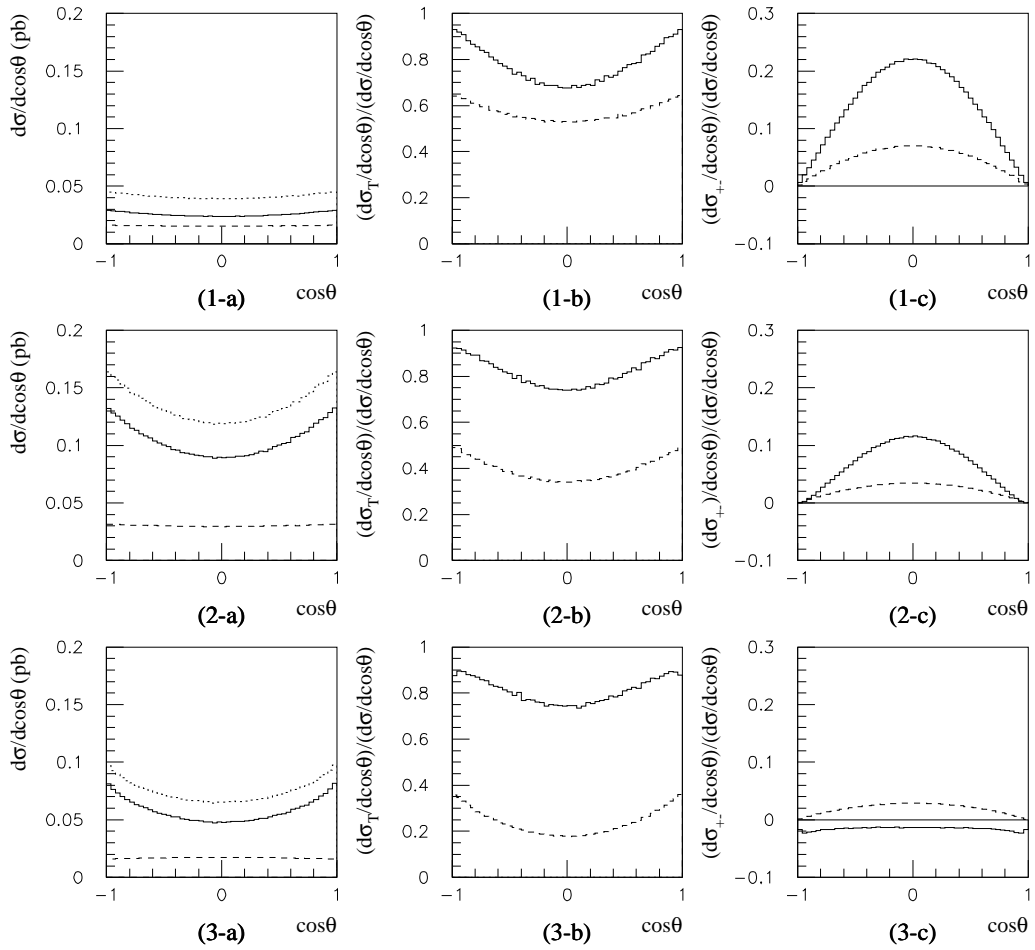


Figure 6: Angular distributions: (1-a,b,c), (2-a,b,c) and (3-a,b,c) are plotted in the intervals $0 \leq z \leq 0.4$, $0.4 < z \leq 0.7$ and $0.7 < z \leq 1$ respectively. (1,2,3-a) are for the total cross section, (1,2,3-b) are for the fraction of the transversely polarized J/ψ and (1,2,3-c) are for the fraction of σ_{+-} . The solid, dashed and dotted lines correspond to the $J/\psi c\bar{c}$, $J/\psi gg$ and total inclusive productions respectively.

distributions on K . In order to give a more direct comparison to the experimental data, we introduce a few kinematic asymmetries. The first one is the observable α defined in Eq. (8), which can be obtained from the J/ψ scattering angle distributions. Although the angular distribution for the QED $J/\psi c\bar{c}$ production is not a standard $1 + \alpha \cos^2 \theta$ function, for comparing with experimental data, we can still use an effective function just like Eq. (8) to fit the curves for the QED mode in the central region, $|\cos \theta| < 0.9$, and then obtain an effective S_{cc}^{QED} and $\alpha_{cc}^{QED\dagger}$. The angular distribution for the QED mode is described effectively by

$$\frac{d^2\sigma_{cc}^{QED}}{dz d \cos \theta} \simeq S_{cc}^{QED}(z)[1 + \alpha_{cc}^{QED}(z) \cos^2 \theta]. \quad (22)$$

Due to the small cross section of the QED $J/\psi c\bar{c}$ and according to the traditional experimental data analysis, the technique is sufficient to give a good accuracy in comparison with the experimental data.

Simply summing over Eqs. (8) and (22), we work out the effective angular coefficients for $J/\psi c\bar{c}$ production and the total inclusive process respectively,

$$\alpha_{cc} = \frac{S_{cc}^{QED} \alpha_{cc}^{QED} + S_{cc}^{QCD} \alpha_{cc}^{QCD}}{S_{cc}^{QED} + S_{cc}^{QCD}}, \quad \alpha = \frac{S_{cc}^{QED} \alpha_{cc}^{QED} + S_{cc}^{QCD} \alpha_{cc}^{QCD} + S_{gg} \alpha_{gg}}{S_{cc}^{QED} + S_{cc}^{QCD} + S_{gg}}. \quad (23)$$

The second observable is relative to the polar angle θ^* in J/ψ leptonic decays. One can integrate over all other parameters but leave only θ^* in Eq. (20), then obtain an reduced formula

$$\frac{d\sigma}{d \cos \theta^*} = S^* [1 + \alpha^* \cos^2 \theta^*], \quad (24)$$

which is analogue to Eq. (8). The coefficient α^* has a simple relation with the total cross section σ and the transverse cross section σ_T :

$$\alpha^* = \frac{-2\sigma + 3\sigma_T}{2\sigma - \sigma_T}. \quad (25)$$

The observables α and α^* versus the K factor for the QCD $J/\psi c\bar{c}$ process are displayed in Fig. 7 in the full momentum spectrum $0 \leq z \leq 1$ (1-a,1-b) as well as in the moderate and large z regions $0.4 < z \leq 0.7$ (2-a,2-b) and $0.7 < z \leq 1$ (3-a,3-b) respectively. The integrated luminosity in the region $0 \leq z \leq 0.4$ at the B factories comes from the off-resonance data and hence is one order smaller than those in the moderate and large z regions. It is hard to measure the observables precisely in $0 \leq z \leq 0.4$, so we do not present them here. The dashed, dotted and solid lines correspond to the $J/\psi c\bar{c}$, $J/\psi gg$ and the total inclusive productions respectively. The α versus K is given in figures (1-a,2-a,3-a). The α parameter for the $J/\psi gg$ contribution (independent of the K factor) is almost zero at all z region,

[†]Here the fitting program PAW (Physics Analysis Workstation) and χ^2 method have been utilized to obtain the α values.

which is consistent with the flat curves for the total distribution cross section in Figs. 5(b) and 6(1-a,2-a,3-a). For the $J/\psi c\bar{c}$ contribution, α is sensitive to the K values, in particular at small K and at large z (3-a), it varies from 0.9 to 0.6 for $1 < K < 5$. This is due to the large QED $J/\psi c\bar{c}$ contribution in large z region. The α parameter for the total inclusive process varies from 0.25 to 0.4 for $0 \leq z \leq 1$ (1-a), from 0.3 to 0.42 for $0.4 < z \leq 0.7$ (2-a), and from 0.32 to 0.52 for $0.7 < z \leq 1$ (3-a). α^* versus K is shown in figures (1-a,2-a,3-a). The α^* parameter for the $J/\psi c\bar{c}$ contribution is about 0.4 at all z region almost independent of K , while for the $J/\psi gg$ contribution it is about -0.5 for $0.4 < z < 0.7$ (2-b), -0.7 for $0.7 < z < 1$ (3-b). For the total inclusive J/ψ process, the α^* is more sensitive to the K factor than the α . It varies from -0.82 to 0.24 for $0 \leq z \leq 1$ (1-b) and $0.4 < z \leq 0.7$ (2-b), and from -0.7 to 0.2 for $0.7 < z \leq 1$ (3-b). We also plot the Belle data with a one-sigma error which fall into the hatched regions. As shown in Fig. 7, our theoretical calculations do not satisfy the current data very well. The data for α are close to the case of $J/\psi c\bar{c}$ only, while for α^* there is a tendency towards the $J/\psi gg$ predictions. However the errors of the experimental data are still large, and more accurate measurements are needed.

The third asymmetry can be obtained by integrating over all other parameters but leave only the azimuthal ϕ^* in Eq. (20) and therefore the off-diagonal density-matrix element σ_{+-} can be measured. From Eq. (20), we find that σ_{+-} is proportional to $\sin^2 \theta^*$. We also notice from Fig. 6 that σ_{+-} is much larger in the small $|\cos \theta|$ region. In order to enhance the signal as large as possible, we impose the angular cuts $|\cos \theta|, |\cos \theta^*| \leq 1/4$, obtaining

$$\frac{d\sigma_{total}}{d\phi^*} \left(|\cos \theta|, |\cos \theta^*| \leq \frac{1}{4} \right) = \frac{1}{512\pi} (94\sigma - 45\sigma_T + 47\sigma_{+-} \cos 2\phi^*). \quad (26)$$

To retain the information of ϕ^* , we split the phase space in terms of ϕ^* into eight parts and integrate over them separately. After recombination of the eight integrations and normalization by the total cross section, the asymmetry is constructed as

$$\begin{aligned} A \left(|\cos \theta|, |\cos \theta^*| \leq \frac{1}{4} \right) &= \frac{\sum_{n=0}^3 \left[\int_{n\pi/2}^{(n/2+1/4)\pi} d\phi^* - \int_{(n/2+1/4)\pi}^{(n+1)\pi/2} d\phi^* \right] \times (d\sigma_{total}/d\phi^*)}{\sum_{n=0}^3 \left[\int_{n\pi/2}^{(n/2+1/4)\pi} d\phi^* + \int_{(n/2+1/4)\pi}^{(n+1)\pi/2} d\phi^* \right] \times (d\sigma_{total}/d\phi^*)} \\ &= \frac{94\sigma_{+-}}{94\pi\sigma - 45\pi\sigma_T}. \end{aligned} \quad (27)$$

The asymmetry A is generally small except at very high z , because $|\sigma_{+-}|$ for the $J/\psi c\bar{c}$ production is quite large near $z \sim 0.9$ which is shown in Fig. 5(e). In Fig. 8, we plot the sensitivity of the K factor for the asymmetry A in the interval $0.85 \leq z \leq 1$. A for the $J/\psi gg$ process (the dotted line) is almost zero while for the $J/\psi c\bar{c}$ (the dashed line) can reach -0.11 . Therefore A for the total inclusive production (the solid line) is sensitive to the K factor due to the enhancement of the $J/\psi c\bar{c}$ component with the increasing K value.

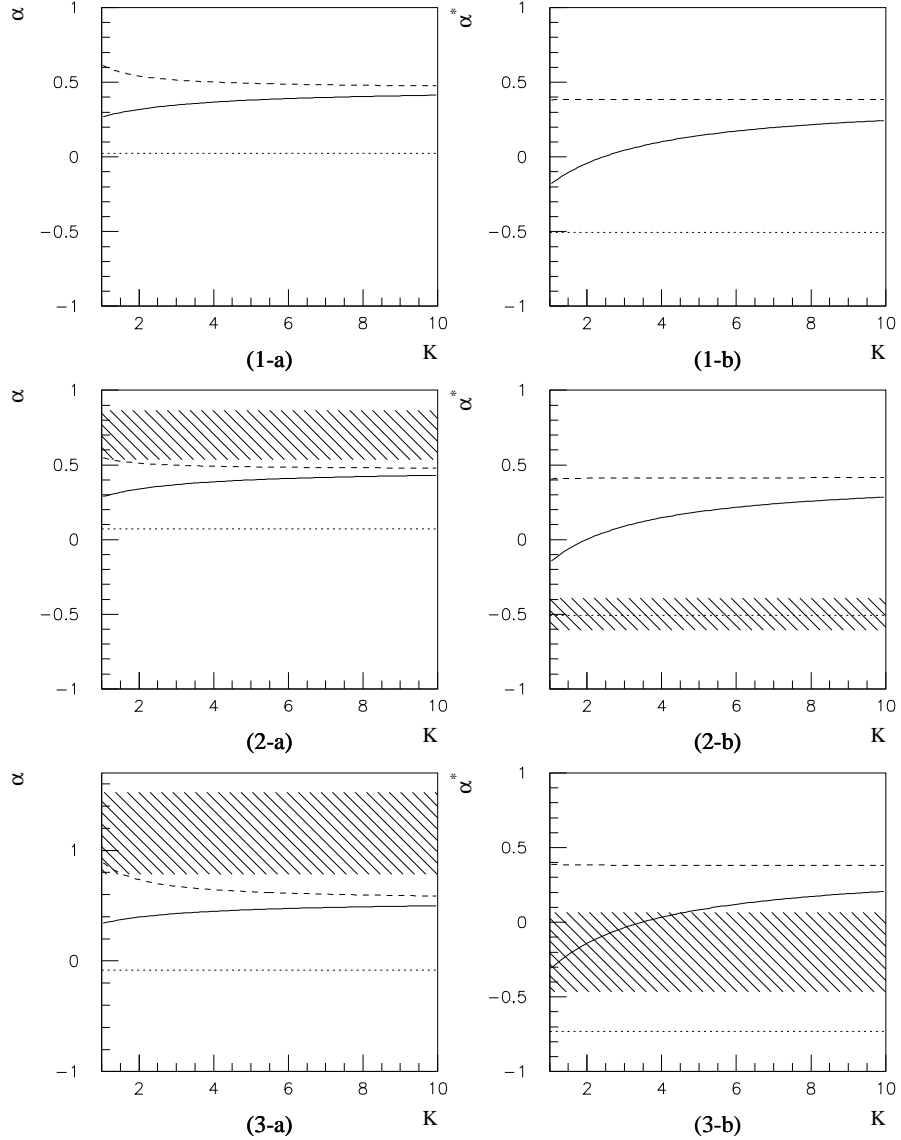


Figure 7: Sensitivity of the K factor for α and α^* : (1-a,b), (2-a,b) and (3-a,b) are plotted in the intervals $0 \leq z \leq 1$, $0.4 < z \leq 0.7$ and $0.7 < z \leq 1$ respectively. (1,2,3-a) and (1,2,3-b) are for various asymmetries α and α^* respectively. The dashed, dotted and solid lines correspond to the $J/\psi c\bar{c}$, $J/\psi gg$ and the total inclusive productions respectively. The experimental data with a one-sigma error fall into the hatched regions.

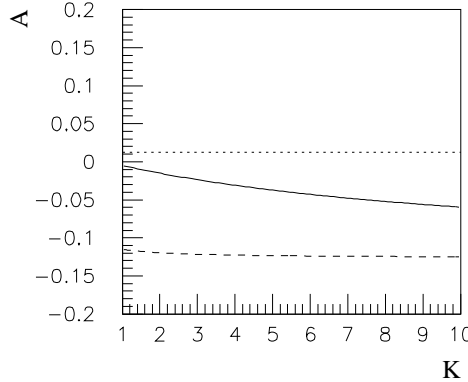


Figure 8: Sensitivity of the K factor for the asymmetry A in the interval $0.85 \leq z \leq 1$. The dashed, dotted and solid lines correspond to the $J/\psi c\bar{c}$, $J/\psi gg$ and the total inclusive productions respectively.

5 Relation between the Inclusive and Exclusive Processes

Since the introduction of the large K factor for the QCD $J/\psi c\bar{c}$ process could provide a reasonable account of the inclusive J/ψ production data, especially the total rate and the $J/\psi c\bar{c}$ fraction, it may also give us a hint of the solution to the puzzle of exclusive $J/\psi \eta_c$ production, where the observed cross section exceeds the NRQCD prediction by one order of magnitude. For instance, the $J/\psi \eta_c$ production cross section can be enhanced by a squared of the K factor for the $J/\psi c\bar{c}$ production process. This can happen if the hard part receives large higher order corrections only when $c\bar{c}$ pair is parallel. Numerically, if we take $K = 4$ for the inclusive production, the K factor for the exclusive one can be as large as 16, which is consistent with the estimate given in Ref. [16].

In the case that J/ψ mesons take maximum momenta in $e^+e^- \rightarrow J/\psi c\bar{c}$ where $c\bar{c}$ pair have the same momentum, the inclusive process matches the exclusive process. Therefore we expect that near the high end point of the J/ψ momentum, the inclusive process should have similar angular distributions with the exclusive one. Notice that Eq. (20) is generally valid for both inclusive and exclusive J/ψ processes. Similar to what has been done in the last section, the angular distribution for $e^+e^- \rightarrow J/\psi \eta_c$ can be expressed as a more definite form [16],

$$\frac{d\sigma}{d \cos \theta d \cos \theta^* d\phi^*} \sim (1 + \cos^2 \theta)(1 + \cos^2 \theta^*) - \sin^2 \theta \sin^2 \theta^* \cos 2\phi^*, \quad (28)$$

where the definitions of θ , θ^* and ϕ^* are the same as in Eq. (20). Comparing the above equation with Eq. (20), we get some general information:

- It is well known that there is no longitudinally polarized J/ψ produced in the exclusive $J/\psi\eta_c$ process due to parity conservation; $\sigma_L/\sigma \rightarrow 0$ in Eq. (21). The feature is also reflected in Eq. (28).
- After integrating over θ^* and ϕ^* in Eq. (28), the total (transverse) cross section σ is proportional to $(1 + \cos^2 \theta)$. It means that the coefficient α defined in Eq. (8) is equal to one in the exclusive limit.
- The nondiagonal density-matrix element σ_{+-} is proportional to $\sin^2 \theta$.
- If the scattering angle θ is fixed at $\pi/2$, the rate for the diagonal and nondiagonal elements, σ_{+-}/σ , can achieve the smallest value -1.

We confirm that the above behaviors are reproduced in the high J/ψ momentum limit of the QCD $J/\psi c\bar{c}$ production cross section. Detailed studies of the inclusive $J/\psi c\bar{c}$ cross section at the highest J/ψ momentum region may reveal the existence of an additional large QCD enhancement factor in the exclusive limit of the process.

6 Conclusions

In this paper, we have calculated the inclusive J/ψ productions in e^+e^- annihilation at the center-of-mass energy 10.58 GeV. Within the framework of NRQCD, we performed the leading-order calculations for the three production modes: the QCD and QED $J/\psi c\bar{c}$ processes and the $J/\psi gg$ process. The cross section ratio for the $J/\psi c\bar{c}$ and $J/\psi gg$ processes is found to be 1:1.5, larger than some previous estimates [4, 5, 6]. In order to explain the Belle experimental data [12, 13, 20], we considered the collinear Sudakov suppression for $J/\psi gg$ and a large renormalization K factor for the QCD $J/\psi c\bar{c}$ mode. We found that our predictions with the K factor of around 4 can reproduce both the inclusive J/ψ momentum distribution and the large fraction of the $J/\psi c\bar{c}$ events [12, 13, 20]. We have presented a complete density-matrix analysis and considered the diagonal elements as well as nondiagonal ones which give rise to polar and azimuthal angle correlations in the J/ψ leptonic decays. The various momentum and angular distributions have been plotted, and their sensitivity to the magnitude of the K factor has been studied. Finally we briefly discussed the relation between the inclusive and exclusive processes.

Throughout this work, we have not presented any discussion on the relativistic corrections to the inclusive J/ψ production. We know that the relativistic corrections may play a very important role since the charm quark is not so heavy and its velocity v is not so small within the charmonium. In fact, with such corrections, the cross section of the exclusive process is doubled [17]. In the case of inclusive processes where only one charmonium is produced, the relativistic corrections should not exceed that for the exclusive one. Therefore if one knows

how large the relativistic corrections affect the total cross section, a significant fraction of the large K factor may be explained.

Before closing the discussion, we note here that we find no evidence of the color-octet contribution to the prompt J/ψ production process. If its contribution is significant, the color-singlet contribution to the $J/\psi gg$ process should be further suppressed in order to keep the large fraction of the $J/\psi c\bar{c}$ process. There is a possibility that the color-octet processes contribute mainly to the ψ' production and that its contribution to direct J/ψ production is suppressed. Detailed studies of prompt J/ψ and ψ' production data in e+e-B factories may reveal the nature of charmonium production dynamics.

Acknowledgments

We would like to thank Bruce Yabsley for discussions about Belle data, and Jun-ich Kanzaki for discussions about the BASES program. ZHL and GHZ thank Ming-Xing Luo for numerous helpful discussions.

The works of KH, ZHL and GHZ are supported in part by Grant-in-Aid Scientific Research from MEXT, Ministry of Education, Culture, Science and Technology of Japan. The works of ZHL and GHZ are supported in part by the Japan Society for the Promotion of Science (JSPS). EK was supported by the Belgian Federal Office for Scientific, Technical and Cultural Affairs through the Interuniversity Attraction Pole P5/27. CFQ is supported in part by the National Science Foundation of China.

Appendix A: Helicity amplitude for NRQCD

In this appendix, we present explicitly how we calculate the helicity amplitudes for NRQCD processes by using the HELAS subroutines [24].

Consider the inclusive production of a quarkonium H with momentum P and helicity λ in colliders, $a + b \rightarrow H_\lambda(P) + X$, where a and b stand for the initial particles which can be e^+e^- or a parton pair and X denotes additional final states. If H is a S -wave bound state, to the lowest order in the velocity v , both quark and anti-quark within the quarkonium are on-shell and carry the momentum $P/2$. Hence the total amplitude can be separated into two independent parts as follows:

$$M(a + b \rightarrow H_\lambda(P) + X) = \sum_{\lambda_1, \lambda_2, i, j} \mathcal{A}(a + b \rightarrow Q_{\lambda_1}^i(P/2) + \bar{Q}_{\lambda_2}^j(P/2) + X) \times \mathcal{F}(Q_{\lambda_1}^i(P/2) + \bar{Q}_{\lambda_2}^j(P/2) \rightarrow H_\lambda(P)), \quad (\text{A.1})$$

where \mathcal{A} is the helicity amplitude in the parton level and \mathcal{F} is the amplitude for forming a bound state. Here $Q(\bar{Q})$ should be charm or bottom quark(anti-quark) with helicity $\lambda_1(\lambda_2)$ and color $i(j)$. The momenta and helicities for the other particles have been suppressed in Eq. (A.1). More explicitly, \mathcal{A} and \mathcal{F} have forms

$$\mathcal{A} = \bar{u}_{\lambda_1}^i(P/2) \Gamma v_{\lambda_2}^j(P/2),$$

$$\mathcal{F} = \bar{v}_{\lambda_2}^j(P/2) \frac{N}{\sqrt{3}} (\gamma_5 \alpha + \not{v}_\lambda(P) \beta) u_{\lambda_1}^i(P/2). \quad (\text{A.2})$$

Here Γ depends on various production processes and has a complicated structure which consists of the wave functions of initial particles a and b as well as the final particles in X . On the other hand \mathcal{F} has a simple structure where $\alpha = 1, \beta = 0$ for pseudo-scalars and $\alpha = 0, \beta = 1$ for vectors. N is a normalization constant related to the meson wave function at the origin $\Psi(0) = R(0)/\sqrt{4\pi}$. The traditional definition of $HQ\bar{Q}$ vertex is given by[26]

$$\frac{\Psi(0)}{2\sqrt{2m}} \frac{\delta_{ij}}{\sqrt{3}} \not{v}_\lambda(P + 2m). \quad (\text{A.3})$$

where m is the heavy quark mass. The above vertex can be obtained identically by contracting $\bar{u}_{\lambda_1}(P/2)$ and $v_{\lambda_2}(P/2)$ in \mathcal{A} with \mathcal{F} and summing over the helicities λ_1 and λ_2 . After simplification of the Dirac matrices, one can find a simple relation between the normalization constant and the wave function

$$N = \frac{\Psi(0)}{(2m)^{3/2}}. \quad (\text{A.4})$$

Both of the amplitudes \mathcal{A} and \mathcal{F} in Eq. (A.2) can be expressed in a transparent manner by using HELAS subroutines. In particular, the program MadGraph can automatically generate a Fortran code for \mathcal{A} such that we only need to write a code for \mathcal{F} and combine \mathcal{A} and \mathcal{F} correctly. After summing over the helicities for the intermediate heavy quark and anti-quark as depicted in Eq. (A.1), we obtain the full amplitude M_λ for different polarized quarkoniums. This M_λ is what we need for calculating the spin density matrix in Sec. 4.

The technique can be utilized also for the quarkonium decay, for instance $J/\psi \rightarrow e^+e^-$. The amplitude has the form

$$M(J/\psi_\lambda(P) \rightarrow e^+e^-) = \sum_{\lambda_1, \lambda_2, i, j} \mathcal{F}(J/\psi_\lambda(P) \rightarrow c_{\lambda_1}^i(P/2) \bar{c}_{\lambda_2}^j(P/2)), \\ \times \mathcal{A}(c_{\lambda_1}^i(P/2) \bar{c}_{\lambda_2}^j(P/2) \rightarrow e^+e^-) \quad (\text{A.5})$$

with

$$\mathcal{F} = \bar{u}_{\lambda_1}^i(P/2) \frac{N}{\sqrt{3}} \not{v}_\lambda(P) v_{\lambda_2}^j(P/2), \\ \mathcal{A} = \bar{v}_{\lambda_2}^j(P/2) \Gamma' u_{\lambda_1}^i(P/2). \quad (\text{A.6})$$

With this amplitude, one can easily obtain the leptonic decay width. By comparing with the analytic formula for the leptonic decay, we verify that our normalization factor N in Eq. (A.4) is correct.

We can also apply the method to calculate the exclusive processes where the additional heavy quark pair should form another quarkonium. The amplitude is expressed as

$$M(a + b \rightarrow H_1^\lambda(P_1) + H_2^{\lambda'}(P_2))$$

$$\begin{aligned}
&= \sum_{\lambda_1, \lambda_2, i, j} \sum_{\lambda_3, \lambda_4, k, l} \mathcal{A}(a + b \rightarrow Q_{\lambda_1}^i(P_1/2) + \bar{Q}_{\lambda_2}^j(P_1/2) + Q_{\lambda_3}^k(P_2/2) + \bar{Q}_{\lambda_4}^l(P_2/2)) \\
&\quad \times \mathcal{F}_1(Q_{\lambda_1}^i(P_1/2) + \bar{Q}_{\lambda_2}^j(P_1/2) \rightarrow H_1^\lambda(P_1)) \\
&\quad \times \mathcal{F}_2(Q_{\lambda_3}^k(P_2/2) + \bar{Q}_{\lambda_4}^l(P_2/2) \rightarrow H_2^{\lambda'}(P_2)),
\end{aligned} \tag{A.7}$$

where the production amplitude is now expressed as

$$\mathcal{A} = \bar{u}_{\lambda_1}^i(P_1/2) \Gamma_1 v_{\lambda_2}^j(P_1/2) \bar{u}_{\lambda_3}^k(P_2/2) \Gamma_2 v_{\lambda_4}^l(P_2/2) \tag{A.8}$$

and \mathcal{F}_1 and \mathcal{F}_2 have similar structures as those in Eq. (A.2) except for different momentum, helicity and color indices. Summation over the helicities and color indices of two pairs of c and \bar{c} wave functions gives the helicity amplitudes for the exclusive process $e^+e^- \rightarrow J/\psi\eta_c$.

References

- [1] G.T. Bodwin, E. Braaten and G.P. Lepage, Phys. Rev. D **51**, 1125 (1995) [Erratum-ibid. D **55**, 5853 (1997)].
- [2] CDF Collaboration, F. Abe *et al.*, Phys. Rev. Lett. **79**, 572 (1997); **79**, 578 (1997).
- [3] E. Braaten and Y.-Q. Chen, Phys. Rev. Lett. **76**, 730 (1993).
- [4] P. Cho and A.K. Leibovich, Phys. Rev. D **54**, 6690 (1996).
- [5] F. Yuan, C.-F. Qiao, and K.-T. Chao, Phys. Rev. D **56**, 321 (1997).
- [6] S. Baek, J. Lee, H.S. Song, and P. Ko, J. Korean Phys. Soc. **33**, 97 (1998); S. Baek, P. Ko, J. Lee, and H.S. Song, hep-ph/9804455.
- [7] C.-H. Chang, C.-F. Qiao, and J.-X. Wang, Phys. Rev. D **56**, 1363 (1997); **57**, 4035 (1998).
- [8] K.-Y. Liu, Z.-G. He, and K.-T. Chao, Phys. Lett. B **557**, 45 (2003).
- [9] K.-Y. Liu, Z.-G. He, and K.-T. Chao, Phys. Rev. D **68**, 031501 (2003).
- [10] A.B. Kaidalov hep-ph/0301246; A.V. Berezhnoy and A.K. Likhoded, hep-ph/0303145; A.V. Luchinsky, hep-ph/0305253; B.L. Ioffe and D.E. Kharzeev, hep-ph/0306062.
- [11] BaBar Collaboration, B. Aubert *et al.*, Phys. Rev. Lett. **87**, 162002 (2001).
- [12] Belle Collaboration, K. Abe *et al.*, Phys. Rev. Lett. **88**, 052001 (2002).
- [13] Belle Collaboration, K. Abe *et al.*, Phys. Rev. Lett. **89**, 142001 (2002).
- [14] S. Fleming, A. K. Leibovich and T. Mehen, Phys. Rev. D **68**, 094011 (2003).

[15] R.Seuster, *Latest results from Belle*, the talk given on 16 - 22 February 2003, Lake Louise, Alberta, Canada; P. Pakhlov, *Measurement of double $c\bar{c}$ production*, the talk given on 22 - 29 March 2003, Les Arcs, France.

[16] K. Hagiwara, E. Kou, and C.-F. Qiao, Phys. Lett. B **570**, 39 (2003).

[17] E. Braaten and J. Lee, Phys. Rev. D **67**, 054007 (2003).

[18] G.T. Bodwin, J. Lee, and E. Braaten, Phys. Rev. Lett **90**, 162001 (2003); Phys. Rev. D **67**, 054023 (2003).

[19] A.V. Luchinsky, hep-ph/0301190.

[20] K. Abe [Belle Collaboration], hep-ex/0306015.

[21] CLEO Collaboration, B. Nemati *et al.*, Phys. Rev. D **55**, 5273 (1997).

[22] C.W. Bauer *et al.*, Phys. Rev. D **64**, 114014 (2001).

[23] S. Fleming and A.K. Leibovich, Phys. Rev. Lett, **90**, 032001 (2003); Phys. Rev. D **67**, 074035 (2003).

[24] H. Murayama, I. Watanabe, and K. Hagiwara, *HELAS: Helicity Amplitude Subroutine for Feynman Diagram Evaluation*, KEK Report 91-11, 1992.

[25] T. Stelzer and W.F. Long, Comput. Phys. Commun. **81**, 357 (1994); F. Maltoni and T. Stelzer, JHEP **0302**, 027 (2003); see also MadGraph homepage, <http://madgraph.physics.uiuc.edu/>.

[26] W.-Y. Keung, Phys. Rev. D **23**, 2072 (1981); J.H. Kühn and H. Schneider, Phys. Rev. D **24**, 2996 (1981); Z. Phys. C **11**, 263 (1981); V.M. Driesen, J.H. Kühn, and E. Mirkes, Phys. Rev. D **49**, 3197 (1994).

[27] S. Kawabata, Comput. Phys. Commun. **88**, 309 (1995).

[28] E.J. Eichten and C. Quigg, Phys. Rev. D **52**, 1726 (1995).

[29] E. Braaten, K. Cheung, and T.C. Yuan, Phys. Rev. D **48**, 5049 (1993).

[30] F. Maltoni and A. Petrelli, Phys. Rev. D **59**, 074006 (1999); I.Z. Rothstein and M.B. Wise, Phys. Lett. B **402**, 346 (1997).

[31] C.W. Bauer *et al.*, Phys. Rev. D **63**, 014006 (2001); C.W. Bauer *et al.*, Phys. Rev. D **63**, 114020 (2001); C.W. Bauer and I.W. Stewart, Phys. Lett. B **516**, 134 (2001); C.W. Bauer *et al.*, Phys. Rev. D **65**, 054022 (2002).

[32] Particle Data Group, K. Hagiwara *et al.*, Phys. Rev. D **66**, 010001 (2002).